Numerical modeling of nonstationary hydrodynamic forces and induced motions of a coupled offshore floating installation system

Shujie Zhao [a], Xun Meng [a], Zhen Gao [b], Huajun Li [a*]

[a] Ocean University of China, Qingdao 266100, China

[b] Department of Marine Technology, Norwegian University of Science and Technology, Trondheim, 7491, Norway

Abstract

Offshore installations always involve multi-body systems in which the hydrodynamic and mechanical interactions are complicated for the properties keep changing under certain operation procedures. Float-over deck (FOD) installation is a typical example, where the draft of barge continuously varies during the load transfer operation. Numerical analysis of such continuous operation is crucial to identify the extreme responses, but it's difficult to model the nonstationary properties involved in the hydrodynamic loads and motions and contact loads of the system. In the study, a numerical modeling methodology is developed to calculate these nonstationary hydrodynamic forces and induced responses, considering an active update of the hydrodynamic properties with the time varying body boundary conditions. The effects of time varying body boundary conditions on hydrodynamic forces and induced nonstationary motions and contact loads of a FOD installation system is studied. The results indicate that the dynamic analysis of the continuous load transfer operation could be effectively carried out with one update of hydrodynamic forces at the end of the operation. The barge roll motions and its natural period are the most affected. The proposed method could be used in intensive simulation of offshore multi-body systems with obvious draft variation during operations.

Keywords

Time varying body boundary conditions; Nonstationary responses; Numerical model; Continuous load transfer operation

1. Introduction

Execution of offshore installation is a critical phase among entire EPCI (engineering, procurement, construction and installation) projects due to the high costs and intensive risky activities (Liu and Li, 2017). It generally includes loadout at the quay, transportation from the quay to the reservoir site, and offshore installation operation in open waters. Because of the complexity of wave forces and multi-body interactions, more attention has been given to the dynamic responses of the structures employed in offshore installations. Intensive motion simulation and load calculation need to be carried out to accurately identify the extreme responses for the success of operation.

One major challenge for analysis of the kind of offshore activities is the reasonable simulation of time varying characteristics during each installation stage, such as the mating process of a float-over deck (FOD) installation (O'neill et al., 2000) or the lowering operation of an offshore wind turbine monopile substructure (Li et al., 2015). Here, a ballasting/de-ballasting operation or lowering operation with specific mechanical components are generally performed, where the mass and the wet surface of the floating body are time varied under random waves. Consequently, the system responses like hydrodynamic forces, motions and contact loads show the nonstationary properties that the mean value or variance are changed during the operation. A methodology to calculate the nonstationary responses of the system needs to be developed.

As for the changes in mass properties, the Simo theory manual provides an efficient point mass simulation method. Additional efforts are focused on the nonstationary hydrodynamic forces with the time varying body boundary conditions. CFD and the direct time domain approach could be used to deal with the problem. While CFD methods cost significant computational efforts to simulate the environmental conditions when taking into account stochastic features (Orihara and Miyata, 2003). Since the viscous effect of large-volume structures such as the FOD operations is ignorable, CFD approach would not be necessary for hydrodynamic analysis here. For the direct time domain approach, numerical calculation of the boundary value problem at each time step is also computationally intensive (Lin, 1990). Therefore, global dynamic analysis using hybrid frequency-time domain approach (Taghipour et al., 2008) with potential flow theory is widely used to analysis marine operations, and in most cases steady-state hydrodynamic load is a matter of expediency to simplify the analysis process.

To carry out the analysis of the continuous operation with the hybrid frequency-time domain approach, there are two different simulation approaches. One is the discrete phase analysis method, in which the nonstationary process is divided into several critical subphases, and the steady-state hydrodynamic forces are considered at each subphase. Koo et al. (2010a, 2010b) carried out numerical simulations and experimental tests for catamaran float-over operations. The premating phase and 0%, 20%, 50%, 80% and 100% load transfer phases were analyzed. Chen et al. (2017) developed a coupled heave-roll-pitch model of FOD system to analyze the complex responses behavior of 0% and 100% load transfer phases. Many software programs like AQWA (Ansys, 2013), Simo (MARINTEK, 2012) and Moses (Nachlinger, 2013) also provides the discrete phase simulations of the nonstationary process.

Another approach is developed under the assumption that the nonstationary process is represented by stepwise steady-state stages (Li et al., 2015). Bai et al. (2021, 2020a) carried out an experimental investigation of the complex continuous load transfer operation of float-over operation. It indicate that continuous transfer modeling could capture variation property of the loads and provide much more reasonable results of the dynamic float-over operation compared with traditional discrete steady-state modeling (Bai et al., 2020b). The continuous operation modeling would be preferred due to the more realistic simulations of the entire nonstationary process.

During the simulations of continuous process, calculation of the nonstationary hydrodynamic forces is crucial. There are few literatures on the action mechanism and realization mode of nonstationary hydrodynamic forces of the complicated offshore floating system in time domain analysis. In the study, a numerical modeling method for assessing of nonstationary hydrodynamic forces and induced motions and contact loads of floating structures in random waves is proposed. Essentially, the method combines the analysis of the operation and the hydrostatic/hydrodynamic loads and motion analysis with time varying body boundary conditions. A case study on float-over installation of a heavy integrated topside is carried out. The effects of time varying body boundary conditions on the hydrostatic restoring forces, wave excitation forces and radiation wave forces are discussed respectively. The corresponding effects on the induced motions and contact loads are also investigated. The paper is organized as follows. Section 2 provides a description of the nonstationary hydrodynamic problems of float-over deck installation. Section 3 elaborates on the developed numerical modeling method to calculate nonstationary hydrodynamic forces and induced responses.

Section 4 and Section 5 present the detailed analysis of the effects of time varying body boundary conditions on system responses. Finally, Section 6 summarizes the conclusions.

2. Nonstationary hydrodynamic problems of FOD installation

Offshore platform mainly consists of a topside and a supporting substructure, which are designed and fabricated separately and integrated together at the site. With the increasing size and weight of the integrated topside, the capacity of the traditional heavy lifting cannot meet the need. The FOD installation technology is preferred for integrated deck operations because of its larger lifting capacity and lower costs. Targeting at the load transfer operation of a single barge FOD installation, a simplified model is illustrated in Fig. 1. All bodies including a barge, a topside and a fixed jacket are considered rigid. The leg mating unit (LMU), the deck support unit (DSU) and the fender components are installed to absorb the impact loads between the bodies.

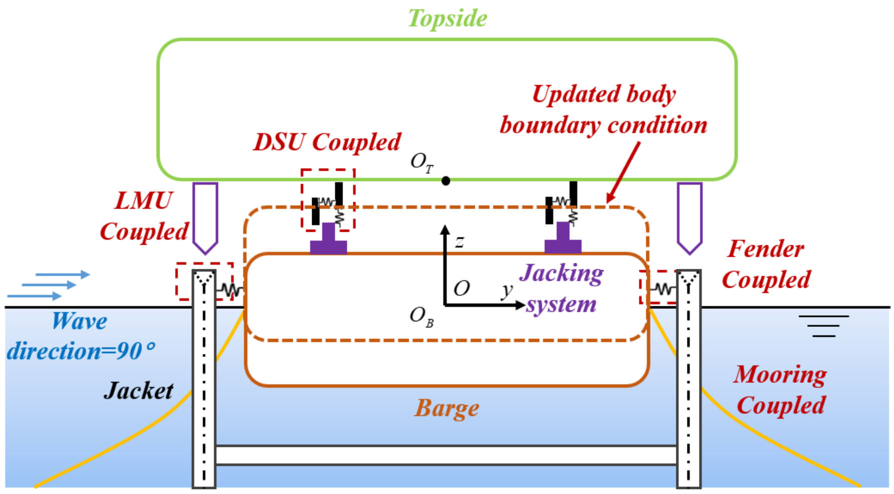

Fig. 1. Load transfer operation of FOD installation

Except for ballast or de-ballast technology, the rapid load transfer technique (Yu et al., 2018) with specific jacking system is used to lower the topsides, where the lowering speed is generally set to 0.25 m/s. During the lowering operation, the draft of float-over barge is decreased as the load of the topside transferring to the substructure, shown as the dotted profile of the floating barge in Fig. 1. The equilibrium for the varying draft with loads transfer is coordinated for each time instant on the hydrostatic and gravitational load as well as quasistatic mooring and contact forces (i.e., forces of the LMU, DSU and fender components). The new equilibrium position implies that all hydrodynamic loads due to waves would be estimated again considering the updated body boundary condition at new quasistatic equilibrium. This kind of hydrodynamic problem is defined as a nonstationary hydrodynamic problem in the study. It is related to a physical process involving a continuous update of the body boundary condition for hydrodynamic analysis under stationary Gaussian random wave processes.

The 12 degree-of-freedom (12-DOF) multi-body motion equations of a barge and a topside, as well as the coupled model of LMU, DSU, fender and jacking components, are developed to carry out the time domain analysis. These model and components particulars were deliberated by Zhao et al. (2021), more efforts are paid on the introduction mechanism of nonstationary hydrodynamic forces and corresponding responses of the multi-body system at rapid load transfer operation.

3. Methodology

A detailed methodology to obtain the nonstationary hydrostatic/hydrodynamic loads considering the FOD operation is developed and explained in this section.

The coordinate system is defined in Fig. 2, where the XY plane of the global Earth-fixed coordinate system $O\text{-}XYZ$ coincides with the still water line and the Z-axis points upwards. The body-fixed coordinate system $\bar{O}\text{-}\bar{X}\bar{Y}\bar{Z}$ follows the motions of the floating body, which is used to describe the positions of the coupling components, such as the mooring system and DSU relative to the floating body. In addition, the body-related coordinate system $O_R\text{-}X_RY_RZ_R$ is defined to calculate the hydrodynamic coefficients, that follows the horizontal equilibrium position of the floating body. At the initial stage, the origin of the defined body-fixed and body-related coordinate system coincides with the global coordinate system.

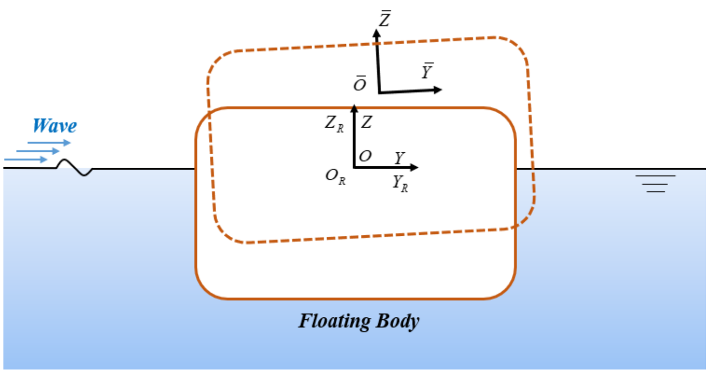

Fig. 2. Definition of the coordinate systems

The rigid-body motions of a floating body with 6 DOFs in waves can be obtained from Newton's second law, as shown in Eq. (1), where $\mathbf{F}_B$ denotes floater position- and orientationdependent buoyancy forces, $\mathbf{F}_M$ denotes mooring forces, $\mathbf{F}_C$ denotes contact forces from LMU, DSU and fender components, $\mathbf{F}_W$ denotes wave excitation forces, $\mathbf{F}_{HS}$ denotes hydrostatic restoring forces due to wave induced body motions, $\mathbf{F}_R$ stands for wave radiation forces corresponding to added mass and potential damping effects, and $\mathbf{F}_G$ is gravity forces of floating body. For the FOD installation with application of the rapid load transfer technique, the ballasting operation is not included during the load transfer phase so that the gravity forces of the float-over barge are considered constant.

$$\mathbf{M}\ddot{\mathbf{x}}(t) = \mathbf{F}_B(t) + \mathbf{F}_M(t) + \mathbf{F}_C(t) + \mathbf{F}_W(t) + \mathbf{F}_{HS}(t) + \mathbf{F}_R(t) + \mathbf{F}_G \tag{1}$$

During the load transfer operation, the float-over barge will move to a new equilibrium position to achieve balance at each time instant as the weight of the topside is gradually transferred. For the developed numerical modeling method, the motions of a floating body of a nonstationary physical process are considered with two parts, as shown in Eq. (2). One is the quasistatic motions $\mathbf{x}_s(t)$ due to the operations in an assumed calm water, and the other is the dynamic motions $\mathbf{x}_d(t)$ with consideration of the wave induced hydrodynamic loads and the inertial loads of the body.

$$\mathbf{x}(t) = \mathbf{x}_s(t) + \mathbf{x}_d(t) \tag{2}$$

Correspondingly, the forces are divided into quasistatic forces and dynamic forces, as shown in Table 1. The hydrodynamic forces are all rewritten as functions of $\mathbf{x}_s$, which means that the forces are calculated based on the boundary condition at $\mathbf{x}_s$. The linear approach to calculate forces is also summarized here, where the term $\bar{\mathbf{K}}$, $\bar{\mathbf{C}}$ and $\bar{\mathbf{M}}$ are the generalized stiffness matrix, generalized damping matrix and generalized mass matrix respectively. Their product with the corresponding motion is the linear calculated forces. It is worth noting that the linear model is only valid for small displacements with respect to the initial linearization point. Nonlinearities are observed for both quasistatic and dynamic forces, as listed in Table 1. In the analysis, the displacements $\mathbf{x}_s$ are large changed with respect to the initial linearization point $\mathbf{x}_s(0)$; therefore, the nonlinear relationships between the load and displacement for quasistatic analysis are captured. While the displacements $\mathbf{x}_d$ are a small value with respect to the new updated quasistatic positions, the linear model in Table 1 is used for the calculation of dynamic forces.

Table 1 Summary of the forces in the numerical model

<table>
<tr><th>Force components</th><th colspan="3">Nature of these forces (quasistatic, dynamic or both)</th><th colspan="2">Linear model for these forces</th><th>Nonlinear model for these forces</th></tr>
<tr><td>$\mathbf{F}_B(t)$</td><td rowspan="3">Quasistatic forces</td><td colspan="2">$\mathbf{F}_B(t)$</td><td colspan="2">$\mathbf{F}_B(t)-\bar{\mathbf{K}}\mathbf{x}_s(t)$</td><td>Buoyancy force considering the instantaneous wet surface due to quasistatic motions</td></tr>
<tr><td>$\mathbf{F}_M(t)$</td><td>$\mathbf{F}_{Ms}(t)$</td><td>$\mathbf{F}_{Md}(t)$</td><td>$\bar{\mathbf{K}}\mathbf{x}_s(t)$</td><td>$\bar{\mathbf{K}}\mathbf{x}_d(t)$</td><td>Nonlinear restoring forces of the mooring lines</td></tr>
<tr><td>$\mathbf{F}_C(t)$</td><td>$\mathbf{F}_{Cs}(t)$</td><td>$\mathbf{F}_{Cd}(t)$</td><td>$\bar{\mathbf{K}}\mathbf{x}_s(t)$
$\bar{\mathbf{C}}\dot{\mathbf{x}}_s(t)$</td><td>$\bar{\mathbf{K}}\mathbf{x}_d(t)$
$\bar{\mathbf{C}}\dot{\mathbf{x}}_d(t)$</td><td>Nonlinear contact forces of stiffness and damping effects</td></tr>
<tr><td>$\mathbf{F}_W(t)$</td><td rowspan="3">Dynamic forces</td><td colspan="2">$\mathbf{F}_W(t,\mathbf{x}_s)$</td><td colspan="2">Refer as Eq. (10)</td><td>Wave excitation force considering the instantaneous wet surface</td></tr>
<tr><td>$\mathbf{F}_{HS}(t)$</td><td colspan="2">$\mathbf{F}_{HS}(t,\mathbf{x}_s)$</td><td colspan="2">Refer as Eq. (11)</td><td>Hydrostatic restoring force considering the hydrostatic pressure integration over the instantaneous wet surface due to dynamic motions</td></tr>
<tr><td>$\mathbf{F}_R(t)$</td><td colspan="2">$\mathbf{F}_R(t,\mathbf{x}_s)$</td><td colspan="2">Refer as Eq. (12)</td><td>Wave radiation force with the radiation wave pressure integration over the instantaneous wet surface</td></tr>
</table>

3.1 Quasistatic analysis of the installation operation

Quasistatic analysis could be executed firstly as Eq. (3). The balance of gravity and equilibrium position-dependent forces (the buoyancy, quasistatic mooring forces and quasistatic lift object contact forces) are accounted to determine the changing quasistatic equilibrium position of the floating body. The changed equilibrium due to the operation are represented by the change of drafts and heeling and trimming angles.

$$\mathbf{0}=\mathbf{F}_B(t)+\mathbf{F}_{Ms}(t)+\mathbf{F}_{Cs}(t)+\mathbf{F}_G \quad (3)$$

As summarized in Table 1, for the mooring system, the restoring forces are modeled considering a nonlinear load-displacement relationship based on a rod theory (Garrett, 1982). The nonlinearity of the contact forces is observed from the nonlinear stiffness and damping properties of components such as DSUs and LMUs. The piecewise linearization of nonlinear stiffness and damping coefficients is used in the simulation. For the position updated buoyancy, nonlinearities are seen from the large varying mean water plane of the floating body during the physical process.

To consider the nonlinearities, the changed buoyancy is evaluated through the integration of pressure p_s on the hull wet surface, shown as Eq. (4).

$$\mathbf{F}_B(t) = \iint_{S_0(\mathbf{x}_s)} p_s \mathbf{n} ds \tag{4}$$

An additional time-updated panel model is required for calculation, which is developed as following three steps.

(a). The whole surface of floating bodies is divided by the quadrilateral element.

(b). For a new static equilibrium position, the coordinates of each node are updated as Eq. (5), where $\boldsymbol{\xi}_s$ and $\boldsymbol{\alpha}_s$ are the quasistatic translational and rotational motion vectors, and $\mathbf{r}$ represents the radius vector for each node.

$$\mathbf{Node}_{i,\mathbf{x}_s} = \mathbf{Node}_{i,\mathbf{x}_{s,0}} + \boldsymbol{\xi}_s + \boldsymbol{\alpha}_s \times \mathbf{r} \tag{5}$$

(c). The last step is to generate a new wet surface mesh. It requires first determining the position of each element relative to the still water, including fully submerged, fully out of water and in between. The last situation requires intercepting the part of an element that is subject to hydrostatic pressure. As shown in Fig. 3 (a), the 'calculation of intersection point' is carried out in a correct way, that requires to calculate the X and Y coordinates of intersection points. While each element is considered small enough, the calculation can be simplified with a 'direct zeroing' procedure as Fig. 3 (b), in which the Z coordinates of each node above the still water is set as zero, and any calculation of other coordinates is not required.

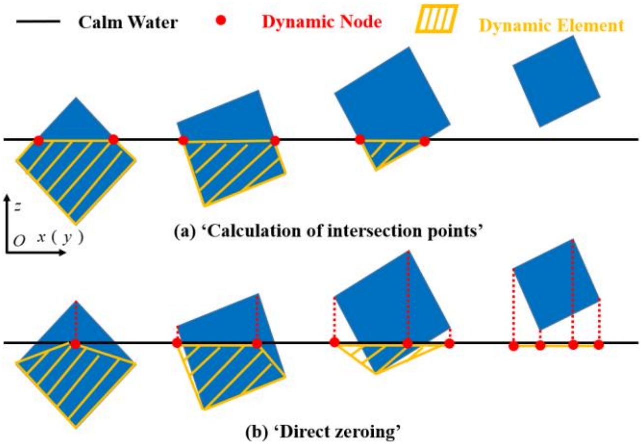

Fig. 3. Time-updated node and panel model

The simplified calculation of intersection points will reduce the computational works, but some errors are also introduced. The accuracy of the procedure to calculate buoyancy needs a verification. As shown in Fig. 4, the buoyancy of two barges with different quasistatic motions is calculated. The verification results listed in Table 2, demonstrate the developed ‘direct zeroing’ procedure as Fig. 3 (b) achieves good agreement with the results integrated on the accurate wet surface as Fig. 3 (a). Besides, because of the largely changed mean water plane of barge 1 at different quasistatic positions, the linear model calculated results have large differences with nonlinear model. It is important to capture the nonlinear relationships between buoyancy and displacement when the mean water plane of the floating body is largely changed.

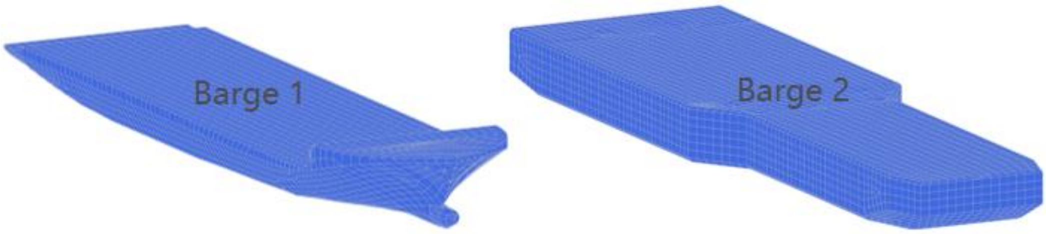

Fig. 4. Discrete panel model of barges

Table 2 Calculated buoyancy with different quasistatic motions

Buoyancy (MN) with different quasistatic Heave (m) and Pitch (deg) motions			(0, 0)	(2, 0)	(0, -3)	(2, -3)
Barge 1	Nonlinear calculation as Eq. (4)	Model as Fig. 3 (a)	184.84	100.45	210.15	125.31
		Model as Fig. 3 (b)	185.56	101.03	211.26	126.27
	Linear calculation as Table 1		184.84	93.72	203.04	111.92
Barge 2	Nonlinear calculation as Eq. (4)	Model as Fig. 3 (a)	671.18	510.41	706.42	545.55
		Model as Fig. 3 (b)	671.20	510.42	707.52	546.64
	Linear calculation as Table 1		671.18	510.30	708.16	547.09

3.2 Dynamic analysis of the installation operation

In the second step, a dynamic analysis is conducted with account of the wave induced hydrodynamic loads acting on the floating body, inertial loads, dynamic forces of the mooring system and contact forces between the structures as Eq. (6).

$$\mathbf{M}\ddot{\mathbf{x}}_d(t) = \mathbf{F}_I(t) + \mathbf{F}_W(t, \mathbf{x}_s) + \mathbf{F}_{HS}(t, \mathbf{x}_s) + \mathbf{F}_R(t, \mathbf{x}_s) + \mathbf{F}_{Md}(t) + \mathbf{F}_{Cd}(t) \quad (6)$$

Here, the quasistatic motions induced inertial force $\mathbf{F}_I$ is included, that could be calculated by interpolation of the determined quasistatic motions defined in Eq. (7). For load transfer operation employing rapid load transfer technique, it plays an important role to reflect the operation induced dynamic responses of the system. Whether the simulation is considered in calm water or waves, the quasistatic motions induced inertial force could be always included. The effects of the forces for barge motions will be discussed in section 4.3.

$$\mathbf{F}_I(t) = -\mathbf{M}\ddot{\mathbf{x}}_s(t) \tag{7}$$

Assuming the speed of quasistatic motions is slow with respect to dominant wave periods, the hydrodynamic loads due to waves can be estimated by interpolation of the wave loads at different body boundary conditions. To carry out the interpolation, the hydrodynamic analysis is conducted in the body-related coordinate system. Due to the fact that the changes in horizontal directions do not cause the changes of wet surface of barge and it is considered as a small value, it is assumed that the equilibrium position change in the horizontal directions is negligible for hydrodynamic analysis. Correspondingly, the body-related coordinate system always coincides with the global coordinate system. The frequency domain hydrodynamic analysis using Wadam (Wadam, 2010) covers the frequency range from 0.02 rad/s to 2 rad/s with a step of 0.02 rad/s. The hydrodynamic coefficients, including hydrostatic restoring coefficients, first-order wave excitation forces, added masses and damping coefficients, are calculated with a step changed drafts of 0.2 m of the floating body and stored in the database. Then the nonstationary hydrodynamic forces and responses of system are calculated as Fig. 5, and each sub-step is illustrated as following.

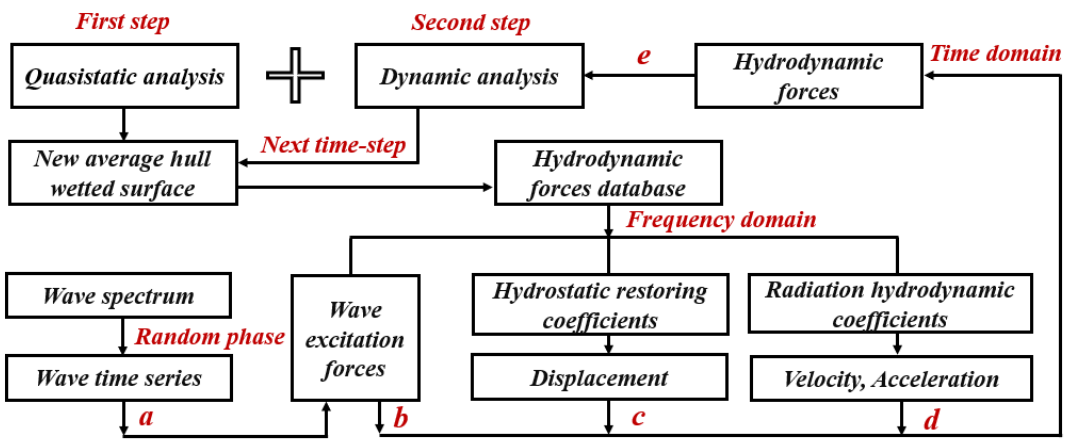

Fig. 5. Hydrodynamic forces and induced motions with time varying body boundary conditions

(a) Environmental conditions for offshore installation works are normally mild; thus, a linear wave theory is used to obtain the wave loads on floating structures (Faltinsen, 1993). The wave spectrum $S(\omega)$ describes the wave condition of offshore operation waters. The random wave elevation time series $\eta(t)$ are generated by superimposing a series of regular wave components with different amplitudes ζ_j, wave frequencies ω_j and random phases ε_j, as shown in Eq. (8) and Eq. (9).

$$\eta(t) = \mathrm{Re}\sum_{j=1}^{N}\zeta_j e^{i(\omega_j t+\varepsilon_j)} \tag{8}$$

$$\zeta_j = \sqrt{2S(\omega_j)\Delta\omega} \tag{9}$$

(b) The wave excitation forces are linearly calculated as Eq. (10), where $f_{Wj}(\omega, \mathbf{x}_s)$ represents the linear wave excitation force transfer functions in the frequency domain at the quasistatic equilibrium position $\mathbf{x}_s$.

$$\mathbf{F}_W(t, \mathbf{x}_s) = \mathrm{Re}\sum_{j=1}^{N}\zeta_j f_{Wj}(\omega, \mathbf{x}_s) e^{i(\omega_j t+\varepsilon_j)} \tag{10}$$

(c) Similar to wave excitation forces, the linearized hydrostatic restoring forces in Eq. (11) are calculated, where $\mathbf{K}_{HS}(\mathbf{x}_s)$ represents the restoring coefficient matrix at quasistatic equilibrium position $\mathbf{x}_s$.

$$\mathbf{F}_{HS}(t, \mathbf{x}_s) = -\mathbf{K}_{HS}(\mathbf{x}_s)\mathbf{x}_d \tag{11}$$

(d) The linear radiation forces are proportional to the acceleration and velocity of dynamic motions $\mathbf{x}_d$, which is calculated using the Cummins equations (Cummins, 1962) as Eq. (12). The time τ is defined as the previous time, and time t is the current time. In Eq. (12), $\mathbf{x}_{s,t}$ and $\mathbf{x}_{s,\tau}$ are the time varying quasistatic equilibrium positions at time instances t and τ respectively, and $\mathbf{A}_\infty(\mathbf{x}_{s,t})$ is the infinite frequency-added mass matrix at $\mathbf{x}_{s,t}$. The convolution term represents the fluid memory effects, and essentially these are the radiation forces at the current time t due to all the waves (or the radiated wave velocity potential) generated by the motions of body at all the previous time instants τ. Since the boundary conditions are different at time τ and t, the calculation becomes complicated:

- The radiated wave velocity potential $\phi^R\left(x, y, z, \mathbf{x}_{s,\tau}\right)$ generated under the previous boundary condition $\mathbf{x}_{s,\tau}$ is calculated, but it should be integrated at the current wet surface $\mathbf{x}_{s,t}$ to obtain the potential damping coefficients $\mathbf{B}(\omega,\mathbf{x}_{s,\tau})$ as Eq. (14). However, the calculated velocity potential is all integrated under its corresponding panel model for hydrodynamic analysis in frequency domain, that is not available for integration as Eq. (14). An approximation method is proposed as Eq. (15), that uses the average of the potential damping coefficients at the quasistatic positions $\mathbf{x}_{s,t}$ and $\mathbf{x}_{s,\tau}$.

- Then the retardation function $\mathbf{K}(t_R,\mathbf{x}_{s,\tau})$ can be calculated by the established relationship by (Ogilvie, 1964) as Eq. (13). With the time t_R shifts, the retardation function will be decayed to near zero, so the retardation function is truncated at 70 s here. And the previous databases of added mass and damping coefficients are re-calculated as Eq. (13)~Eq. (15) and stored as retardation function in the database.

$$\mathbf{F}_R(t,\mathbf{x}_s) = -\left\{ \mathbf{A}_\infty(\mathbf{x}_{s,t})\ddot{\mathbf{x}}_d(t) + \int_{-\infty}^{t} \mathbf{K}(t-\tau,\mathbf{x}_{s,\tau})\dot{\mathbf{x}}_d(\tau,\mathbf{x}_{s,\tau})d\tau \right\} \tag{12}$$

$$\mathbf{K}(t_R,\mathbf{x}_{s,\tau}) = \frac{2}{\pi}\int_0^\infty \mathbf{B}(\omega,\mathbf{x}_{s,\tau})\cos(\omega t_R)d\omega \tag{13}$$

$$\mathbf{B}(\omega,\mathbf{x}_{s,\tau}) = \mathrm{Im}\left(\omega\rho \iint_{S_0(\mathbf{x}_{s,t})} \phi^R\left(x,y,z,\mathbf{x}_{s,\tau}\right)\mathbf{n}\ ds \right) \tag{14}$$

$$\mathbf{B}(\omega,\mathbf{x}_{s,\tau}) = \mathrm{Im}\left(0.5\omega\rho(\iint_{S_0(\mathbf{x}_{s,\tau})} \phi^R\left(x,y,z,\mathbf{x}_{s,\tau}\right)\mathbf{n}\ ds + \iint_{S_0(\mathbf{x}_{s,t})} \phi^R\left(x,y,z,\mathbf{x}_{s,t}\right)\mathbf{n}\ ds) \right) \tag{15}$$

(e) The mass matrix is updated to the established body-related coordinate system as Eq. (16) and Eq. (17), where (x_g, y_g, z_g) is the vector of the center of gravity at the initial quasistatic position, and (x_s, y_s, z_s) is the vector of the quasistatic motions and R_g is the inertia radius.

$$\begin{cases} x_{gs} = x_g + x_s \\ y_{gs} = y_g + y_s \\ z_{gs} = z_g + z_s \end{cases} \tag{16}$$

$$\mathbf{M}=m\begin{bmatrix} 1 & 0 & 0 & 0 & z_{gs} & -y_{gs} \\ 0 & 1 & 0 & -z_{gs} & 0 & x_{gs} \\ 0 & 0 & 1 & y_{gs} & -x_{gs} & 0 \\ 0 & -z_{gs} & y_{gs} & R_{gxx}^2+y_{gs}^2+z_{gs}^2 & R_{gxy}^2-x_{gs}y_{gs} & R_{gxz}^2-x_{gs}z_{gs} \\ z_{gs} & 0 & -x_{gs} & R_{gxy}^2-x_{gs}y_{gs} & R_{gyy}^2+x_{gs}^2+z_{gs}^2 & R_{gyz}^2-y_{gs}z_{gs} \\ -y_{gs} & x_{gs} & 0 & R_{gxz}^2-x_{gs}z_{gs} & R_{gyz}^2-y_{gs}z_{gs} & R_{gzz}^2+x_{gs}^2+y_{gs}^2 \end{bmatrix} \tag{17}$$

Finally, the system motion and contact forces during the continuous operation could be obtained from the addition of calculated quasistatic and dynamic responses.

4. Response analysis of nonstationary responses during the installation operation

Since the nonstationary hydrodynamic forces and nonlinear stiffness of LMU and DSU are acting in the studied continuous operation, the convergence simulation is launched with consideration of the whole load transfer operation with varying time steps. The 4th-order Runge-Kutta numerical method is applied to drive the time-domain responses. The random wave condition of Jonswap spectrum with a significant wave height (*Hs*) of 1.5 m and spectral peak period (*Tp*) of 6.7 s in head sea is employed here. Fig. 6 shows the heave motions of the float-over barge with different time steps. The converged results can be obtained with a time step of 0.01 s, which is adopted for the follow-up time domain simulations. The simulations are carried out on a personal computer (AMD Ryzen 5 4600H@3.0 GHz 4.8 GHz Turbo, 16 GB of RAM). It costs 906 s for a 300 s time series simulation with a time step of 0.01 s.

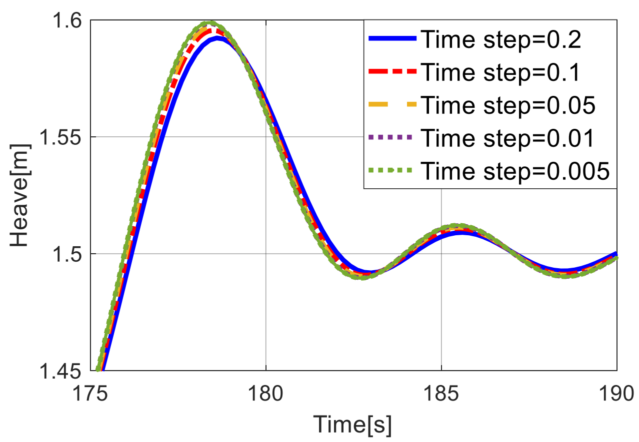

Fig. 6. Heave motions of float-over barge with different time steps

4.1 Properties of float-over barge at the initial and last operation positions

The changed properties of float-over barge before and after load transfer are summarized in

Table 3. The weight of the topside is 10000 t in analyzed FOD installation operation, which is the difference of total mass of barge before and after load transfer. The offloading weight to substructures leads to the changes of draft and trim angle of the barge. In terms of the natural vibration periods, there are small differences of those in heave and pitch motions at the initial and last operation phase, while large changes are observed in roll motions.

Table 3 Properties of float-over barge with varying quasistatic positions

Properties		Before load transfer	After load transfer
Total Mass [t]		68489	58489
Draft [m]		8.55	7.04
Trim [deg]		0	-1.87
Natural period [s]	Heave	9.2	9.1
	Roll	11.4	10.2
	Pitch	10.1	10.0

4.2 Quasistatic motions of float-over barge

Using the verified ‘direct zeroing’ procedure to generate new wet surface mesh, the changed quasistatic motions of the barge with the representation of changed drafts and trim angles are calculated. Based on the average of 10 times calculation of quasistatic motions of barge, the simplified ‘direct zeroing’ process saves 18.1% of the calculation time compared to the ‘ calculation of intersection points’. The results are listed in Table 4. The load transfer operation begins at 150 s, and the first 8 s is to reduce the clearance and the vertical height of docking cones. In this period, the floating condition of the barge is unchanged because the weight of the topside is still fully supported by the barge. After that, the drafts and trim angles of the barge are reduced with the load transferring from the barge to the substructure.

Table 4 Floating condition of float-over barge during load transfer operation

Time [s]		0~158	160	165	170	175	178~End
Floating Condition	Draft [m]	8.550	8.360	7.886	7.474	7.109	7.039
	Trim [deg]	0.000	-0.212	-0.744	-1.260	-1.767	-1.865

4.3 Effects of quasistatic motions induced inertial force

Once the quasistatic motions are determined, the quasistatic motions induced inertial force could be calculated. The simulations are carried out in calm waters. Fig. 7 shows the results of the effect of barge quasistatic motions induced inertial force. It is observed that both heave and pitch motions are increased at the end of the load transfer operation considering of inertial loads. They should not be neglected in analysis of rapid load transfer operation.

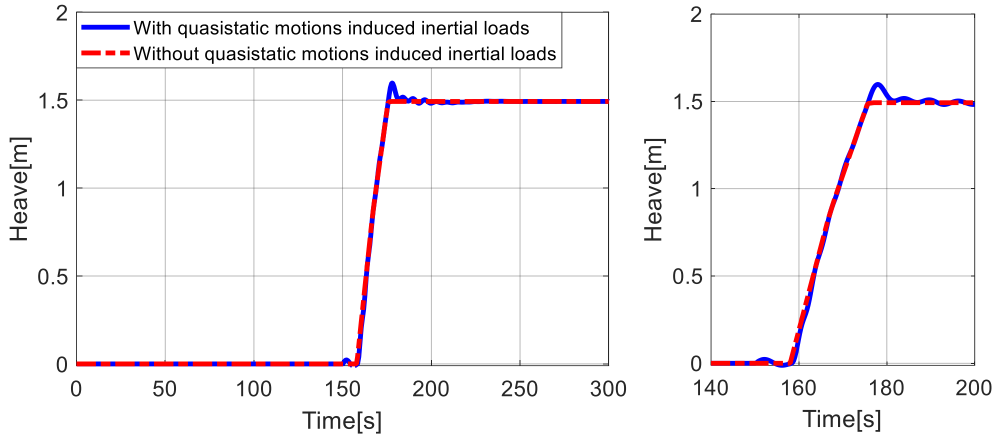

(a) Heave motion of float-over barge

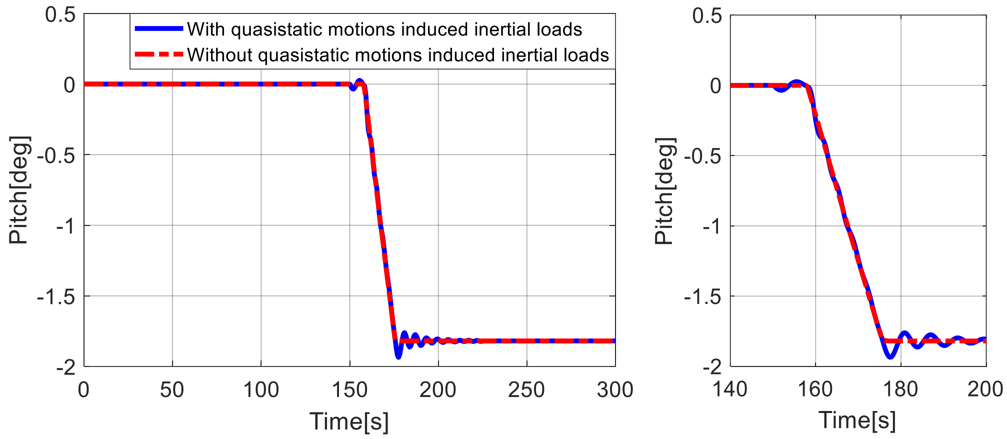

(b) Pitch motion of float-over barge

Fig. 7. Effects of quasistatic motions induced inertial force

5. Effects of hydrodynamic forces with time varying body boundary conditions

The hydrodynamic forces acting on the floating body include hydrostatic restoring forces, wave excitation forces and radiation wave forces. The effects of the time varying body boundary conditions for different hydrodynamic forces are different from one another. In this section, the nonstationary hydrodynamic forces and induced dynamic motions and contact loads are investigated.

5.1 Simulation settings

Calculation settings of hydrostatic and hydrodynamic coefficients considering different body boundary conditions are listed in Table 5.

Table 5 Definition of cases with respect to different modeling methods for hydro forces

Method	Description
C	The calculation is carried out with constant hydro coefficients at the initial floating position.
NHS	The calculation is carried out with nonstationary hydrostatic restoring forces as Eq. (11) and constant wave excitation and radiation coefficients at the initial floating position.
NHS+ NFW	The calculation is carried out with nonstationary hydrostatic restoring forces as Eq. (11) and nonstationary wave excitation forces as Eq. (10), and constant radiation coefficients at the initial floating position.
NHS+ NFW+ NFR	The calculation is carried out with nonstationary hydrodynamic forces as Eq. (10)~Eq. (12) with continuous updated boundary conditions.

Jonswap spectrum with 3 typical peak periods in both head sea (forward along the X axis) and beam sea (forward along the Y axis) are considered. The main parameters of wave conditions are listed in Table 6.

Table 6 Main parameters of the considered sea states

Condition		C1	C2	C3
Tp [s]		6.7	10	14
Hs [m]	Head sea	1.5		
	Beam sea	0.5		

5.2 Hydrodynamic forces of float-over barge with time varying body boundary conditions

5.2.1 Hydrostatic restoring forces

Fig. 8 shows the normalized hydrostatic restoring coefficients during the load transfer operation based on the value of the initial quasistatic equilibrium position. The results show obvious changes in roll direction compared with the hydrostatic restoring coefficients in heave and pitch directions.

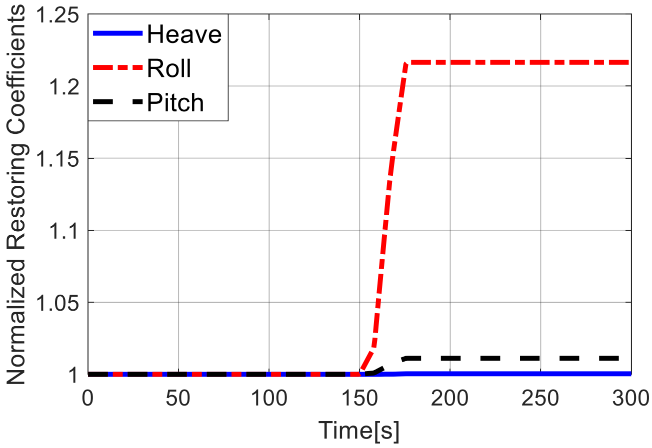

Fig. 8. Normalized hydrostatic restoring coefficients with load transfer operation

The hydrostatic restoring coefficients of roll and pitch motions are calculated as Eq. (18), where V is displacement of float-over barge, z_V is the center of buoyancy, M_B and M_T are the mass of float-over barge and the topside respectively, z_{gB} and z_{gT} are the center of mass of float-over barge and topside, I_{xx} and I_{yy} are the second moment about X-axis and Y-axis over the waterplane area. During the load transfer operation, the second moment I_{xx} changes little, but the changes in the center of mass and buoyancy lead to a great increase in the hydrostatic restoring coefficient for roll motions. As for pitch motions, I_{yy} is far larger than the others in equation because the barge is similar to a slender structure, there is no significant variation in the hydrostatic restoring coefficient for pitch motions.

$$\begin{aligned} K_{HS}(roll, roll) &= \rho g V z_V - (M_B + M_T) g \frac{M_B z_{gB} + M_T z_{gT}}{M_B + M_T} + \rho g I_{xx} \\ K_{HS}(pitch, pitch) &= \rho g V z_V - (M_B + M_T) g \frac{M_B z_{gB} + M_T z_{gT}}{M_B + M_T} + \rho g I_{yy} \end{aligned} \tag{18}$$

5.2.2 Wave excitation forces

The wave excitation forces are related to the incident waves and response amplitude operator (RAO) of forces of float-over barge, that are shown in Fig. 9 and Fig. 10 in head sea and beam sea. The results shows that the effects of the time varying body boundary condition are varied with different wave period. For surge wave excitation forces, the different change tendency is observed among the analyzed wave period. For heave, pitch and roll wave excitation forces, it shows that there is a minimum change between two boundary conditions when long period waves (for most is wave period larger than 12 s) are considered. Besides, the results also illustrate that the changes of wave excitation forces in beam sea are larger than those in head sea. Especially for heave and pitch forces in head sea, the differences are small with two boundary conditions. The heave and pitch forces between 0.5 rad/s and 1 rad/s are magnified to see the changes.

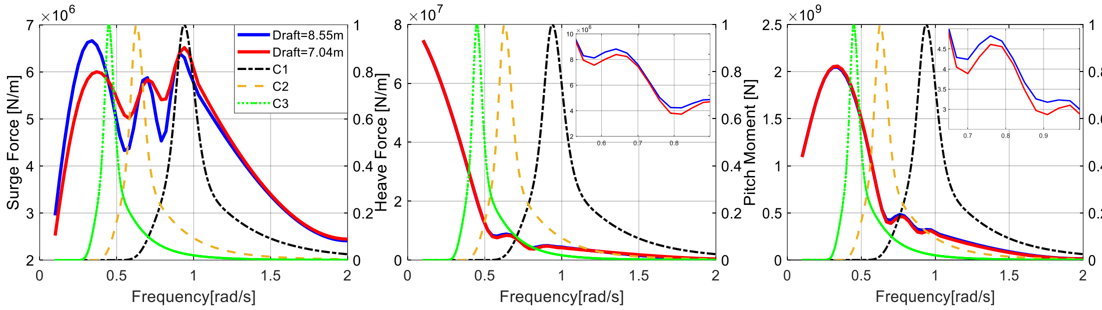

Fig. 9. Wave excitation forces in head sea at the initial and last quasistatic positions

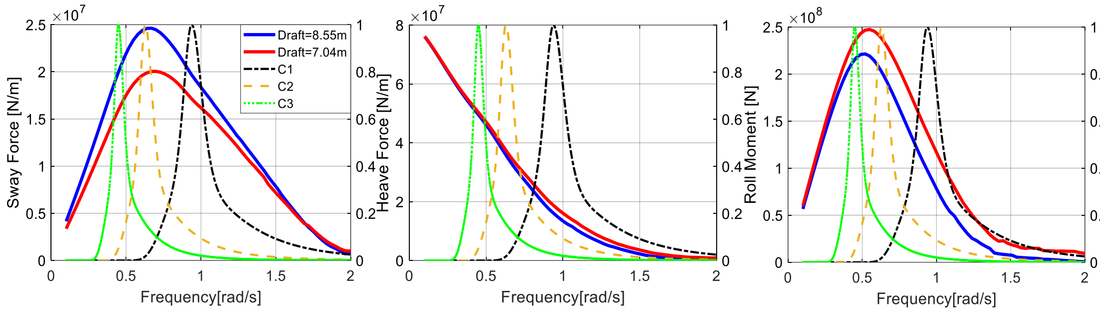

Fig. 10. Wave excitation forces in beam sea at the initial and last quasistatic positions

The time series of constant wave excitation forces (using constant wave excitation force coefficients at the initial floating position) and nonstationary wave excitation forces (using time updated wave excitation force coefficients) in head sea and beam sea are shown in Fig. 11 and Fig. 12. The time series are clarified into load transferring process and after load transfer process. It illustrates that wave excitation forces change little during the load transfer operation while the difference becomes large when the load transfer ended. Because the installation is carried out with the application of the rapid load transfer technique, the load transfer operation only lasts approximately 20 s (158 s~178 s) so that the effects of the time varying boundary conditions could not be observed in a limited time history. Although the frequency domain wave excitation forces coefficients change little for heave and pitch motions, the large differences are still observed in time domain.

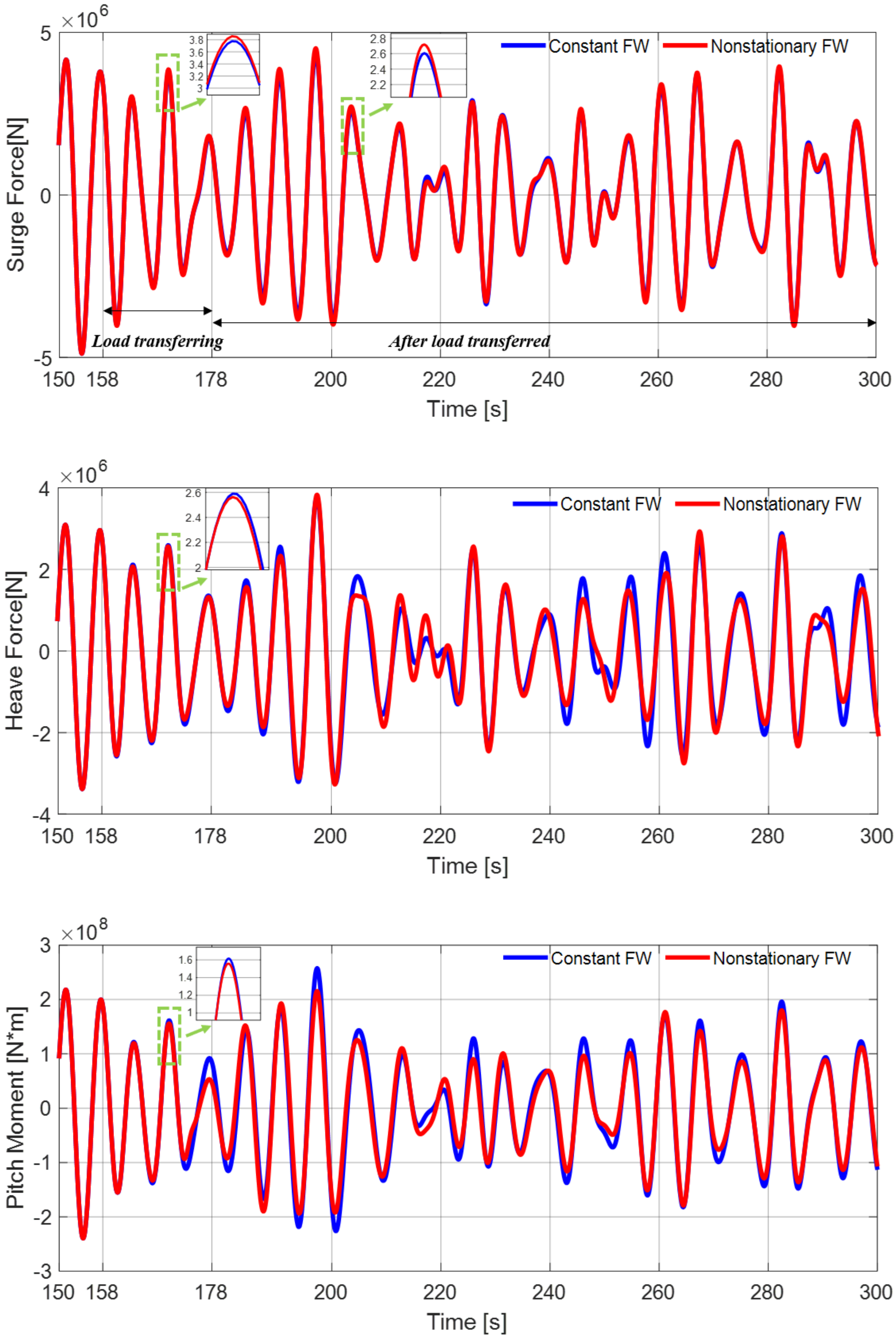

Fig. 11. Wave excitation forces in head sea (Hs=1.5 m, Tp=6.7 s)

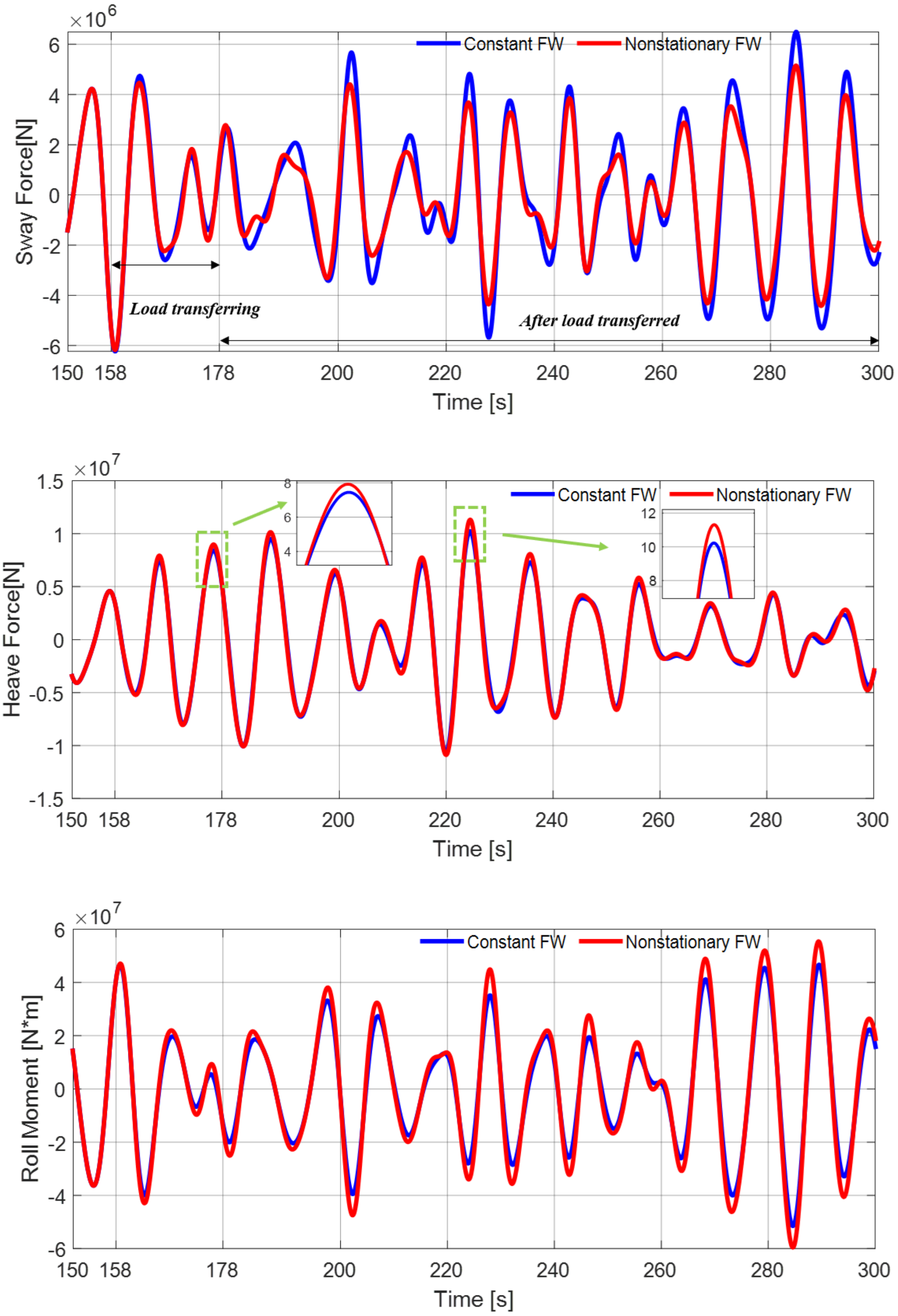

Fig. 12. Wave excitation forces in beam sea (Hs=0.5 m, Tp=10 s)

5.2.3 Radiation wave forces

The radiation forces are represented by the infinite frequency added mass and retardation functions in time domain. Fig. 13 shows the infinite frequency added mass during the load transfer operation, which is normalized based on the value of the initial quasistatic equilibrium position. The changed body boundary condition affects the infinite frequency added mass for surge and sway motions most, and only the infinite frequency added mass for roll motions is increased. It is different for those in other freedoms.

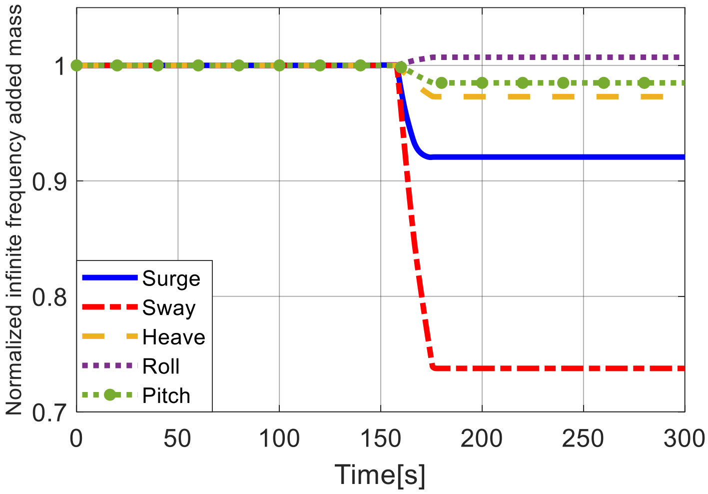

Fig. 13. Normalized infinite frequency added mass with the load transfer operation

In Fig. 14, the retardation functions at different drafts of float-over barge are compared. For surge and sway motions, the retardation functions have the same decrease tendency as the infinite frequency added mass. This will lead the increase of surge and sway motions. Different from the decreases of infinite frequency added mass for heave and pitch motions, the retardation functions are increased considering the changed body boundary condition.

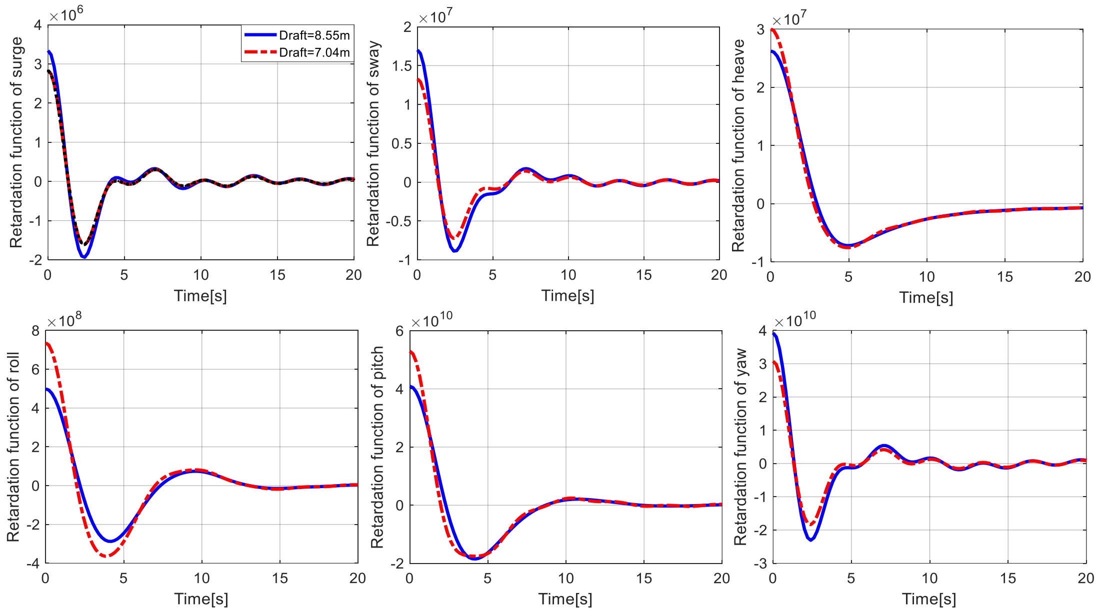

Fig. 14. Retardation functions at different drafts

5.3 Motion comparison

Fig. 15 and Fig. 16 show the dynamic motions of the barge with different hydrodynamic modeling methods in head sea and beam sea. The magnified results of all motions of the barge during the load transfer operation and after load transfer show the same change tendency under the effects of the nonstationary hydrodynamic forces. Same as the changes in wave excitation forces, all the motions of the barge also change little during the load transfer operation. But when the load transfer ended, a larger difference is observed for all motions of the barge. The roll motion is the most affected with the nonstationary hydrodynamic forces, including both motion amplitudes and periods.

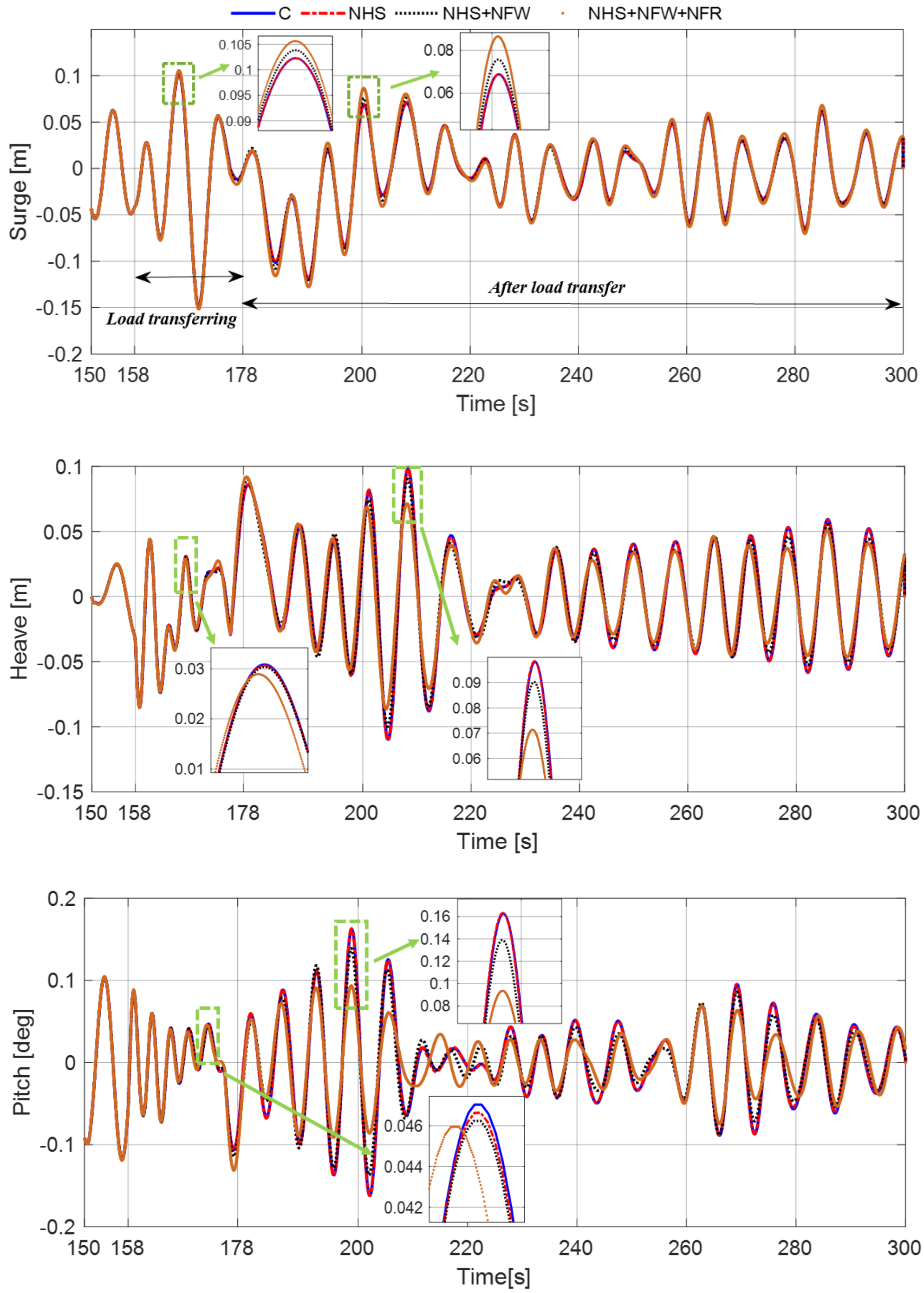

Fig. 15. Dynamic motions of float-over barge in head sea (*Hs*=1.5 m, *Tp*=6.7 s)

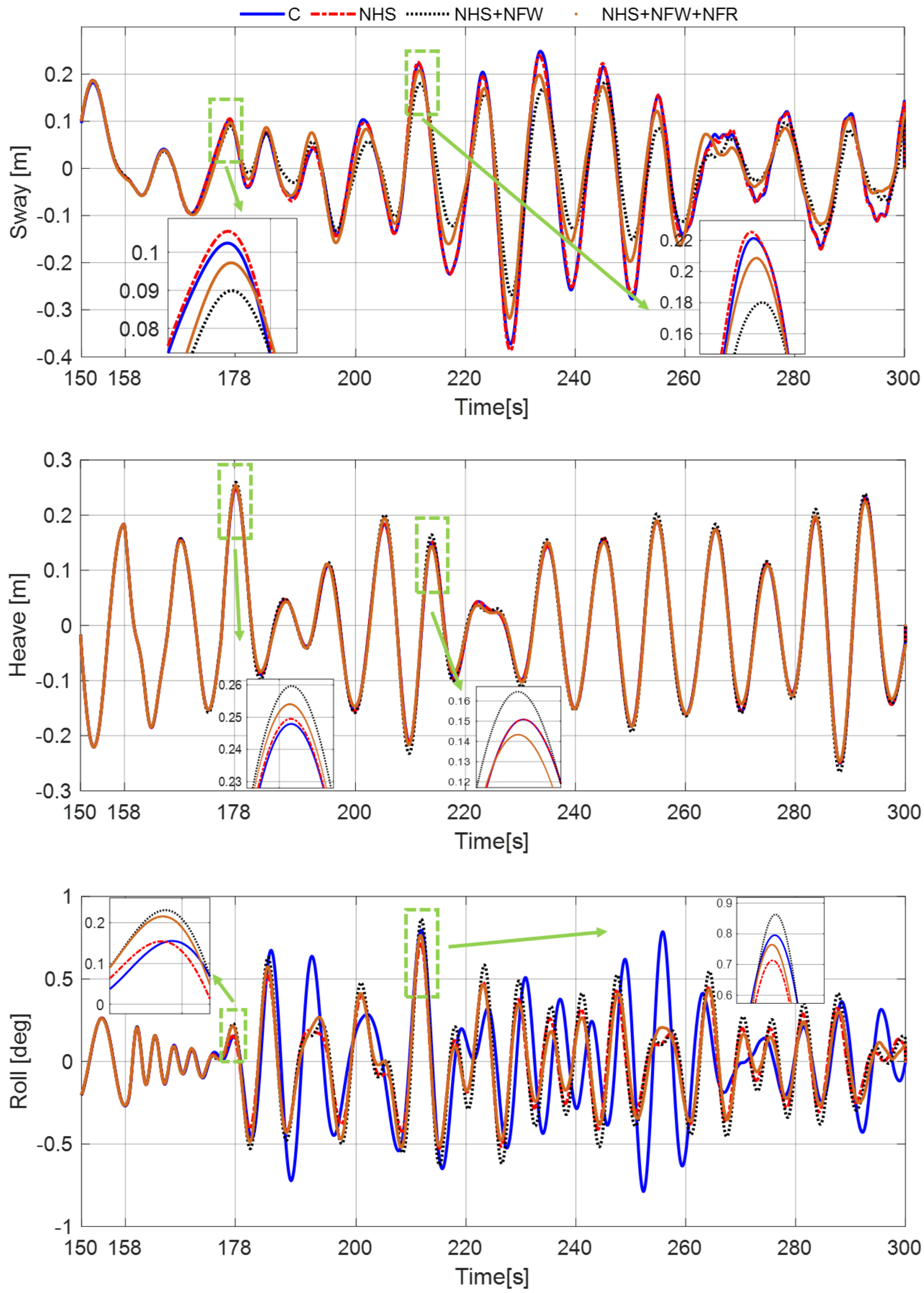

Fig. 16. Dynamic motions of float-over barge in beam sea (Hs=0.5 m, Tp=10 s)

To consider the variability of stochastic waves, 20 times realization of irregular waves are conducted for sea states in Table 6. For each realization, the same wave time series are ensured for the calculation model set in Table 5. The statistical results of barge motions during the load transfer operation and after load transfer in head sea and beam sea are shown in Fig. 17 and Fig. 18. The mean value of the maximum of 20 simulations are used to represent the system statistical results.

The relative variations between different hydrodynamic modeling methods are given in right axis in figure. It further explains the different effects of nonstationary hydrostatic restoring forces, nonstationary wave excitation forces and nonstationary radiation wave forces respectively.

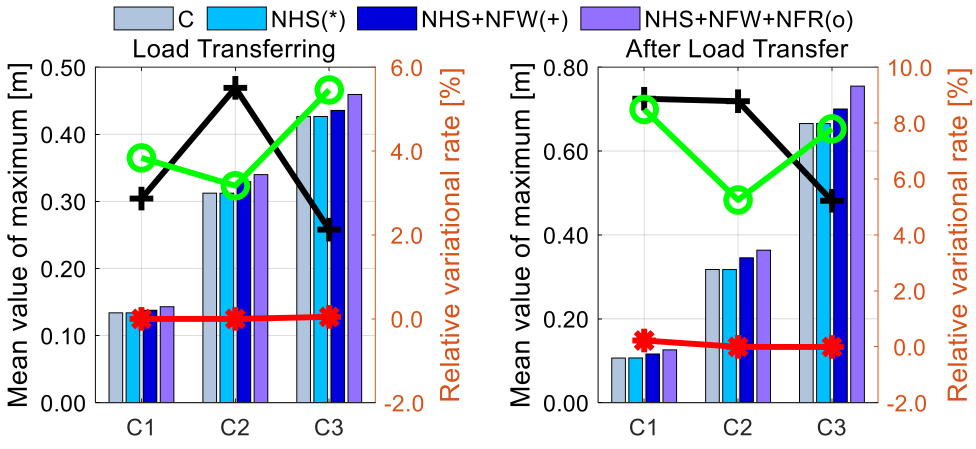

(a) Surge motions

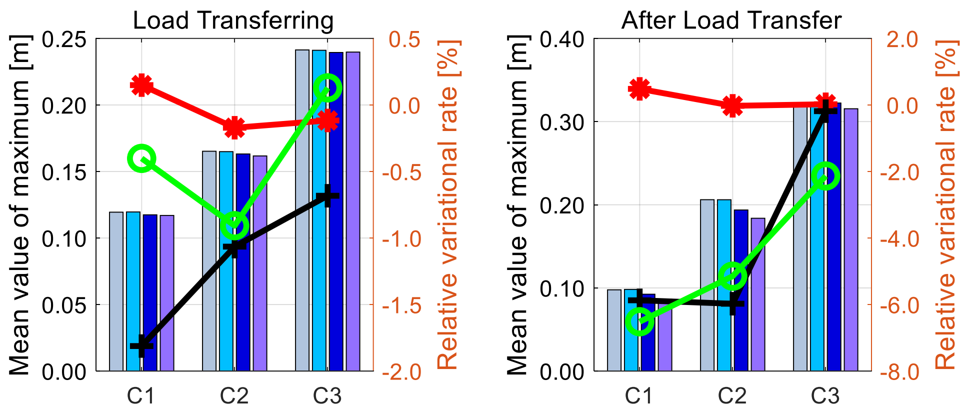

(b) Heave motions

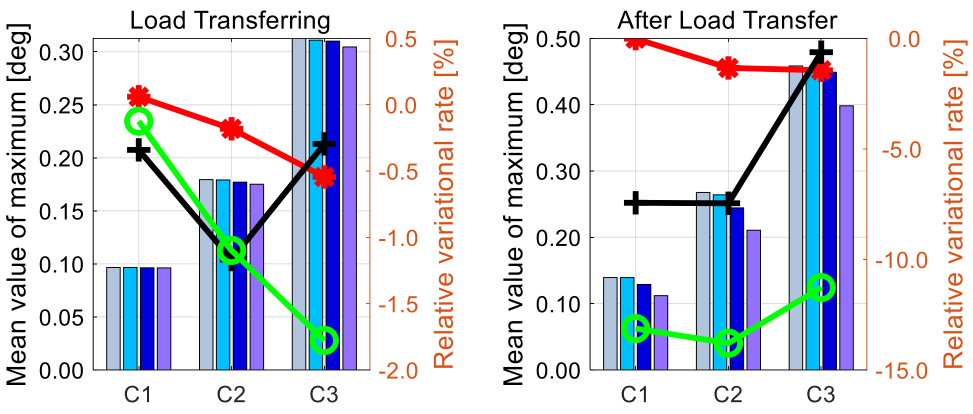

(c) Pitch motions

Fig. 17. Statistical responses in head sea

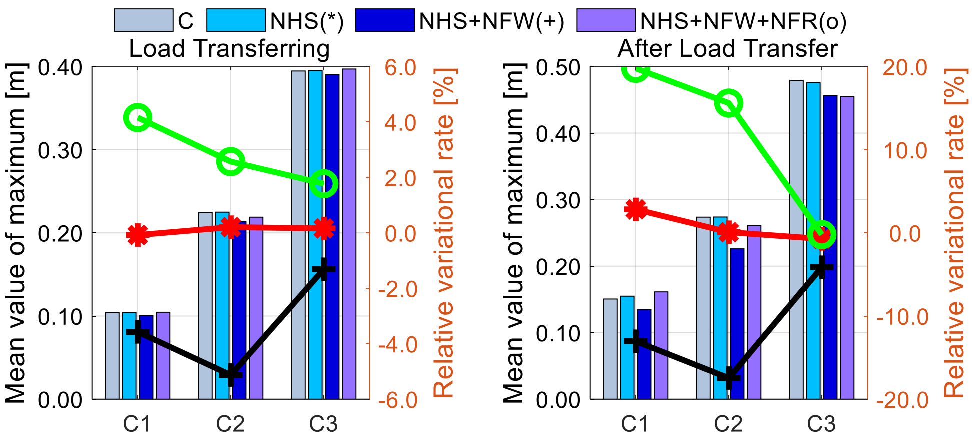

(a) Sway motions

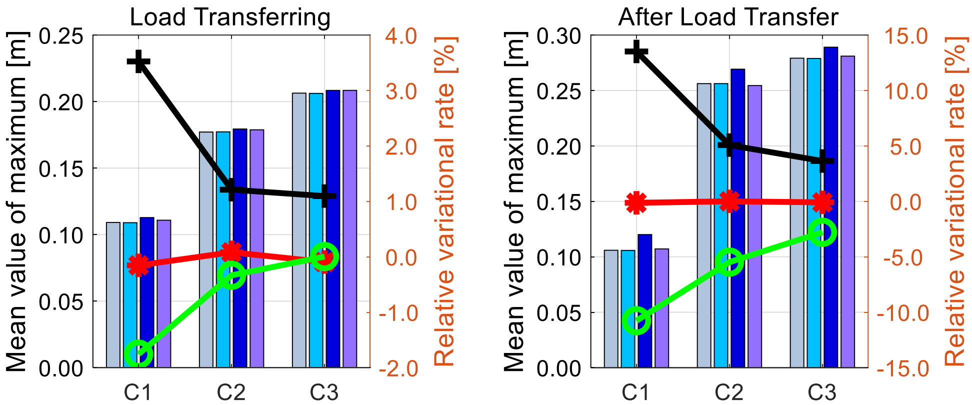

(b) Heave motions

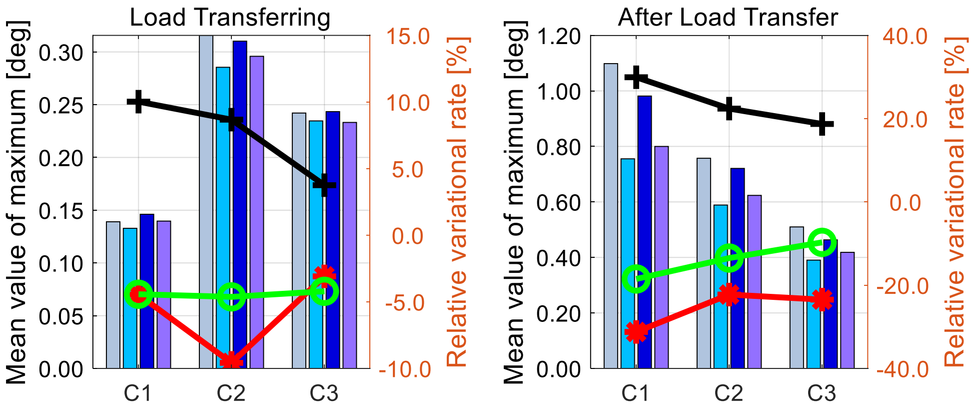

(c) Roll motions

Fig. 18. Statistical responses in beam sea

From Fig. 17 and Fig. 18, the statistical results of the motions of float-over barge are agree with the time history results shown as Fig 15 and Fig 16. It is noteworthy that all motions have a significant change under the effects of nonstationary forces after the operation, while the largest variation of motions during load transfer process is approximately within 5% except for roll motion.

The relative variation rate of roll motions could reach 10% at load transfer process and 30% after load transfer process. In summary, the effects of nonstationary hydrodynamic forces are both observed for the analyzed load transfer operation and after load transfer operation. Based on the methodology proposed, the reasonable dynamic analysis could be simply carried out with one update of hydrodynamic forces at the end of the rapid load transfer operation.

Besides, the nonstationary hydrostatic restoring forces only take effects on the roll motions, and the roll motions are also most affected by the nonstationary wave excitation and radiation forces among all wave induced motions. The attention is also paid to the effects of nonstationary wave excitation forces on motions, that is shown as mark '+' in figures. Previously, it has been concluded that there is a minimum change for heave, pitch and roll wave excitation forces when a long period waves are considered. The heave, pitch and roll motions of barge also show a same change.

5.4 Contact forces

There are 6 sets of DSUs and LMUs used for the FOD installation, and they play the most important role in reducing the impact loads acting on the barge and topside. The statistical vertical contact forces of one represented DSU and LMU that support the maximum weight of the topside are illustrated in Fig. 19~Fig. 20. When the load transfer is ended, there are no more dynamic contact forces between bodies so only the results during the operation are shown in figures. Like the motion responses, the statistical results of the contact forces show same change tendency as motions. In head sea, the contact forces of the DSU and LMU decrease under the effects of nonstationary wave excitation forces and radiation wave forces, and the heave and pitch motions of the barge in Fig.17 (b) and Fig.17 (c) are also decreased. In beam sea, the nonstationary wave excitation forces lead an increase on heave and roll motions, and the nonstationary radiation wave forces lead a decrease of same motions. Correspondingly, the contact forces of DSU and LMU as Fig. 19 and Fig. 20 show the same changes as motions in beam sea.

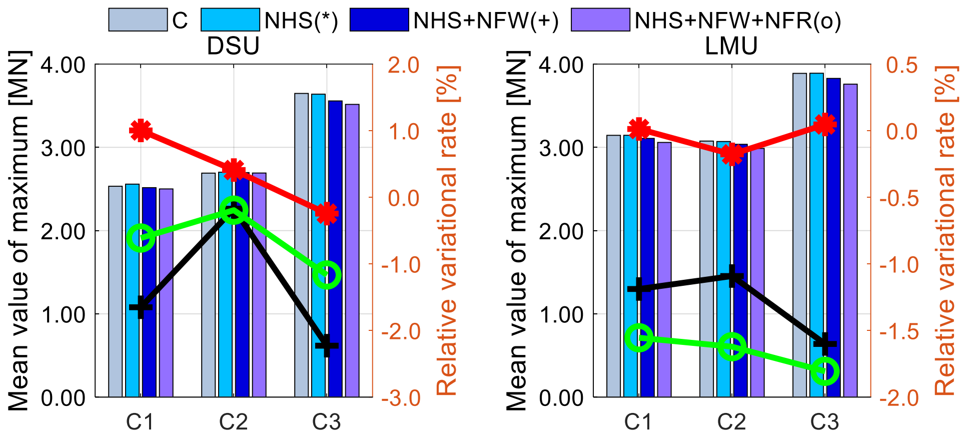

Fig. 19. Statistical vertical forces of DSU and LMU in head sea

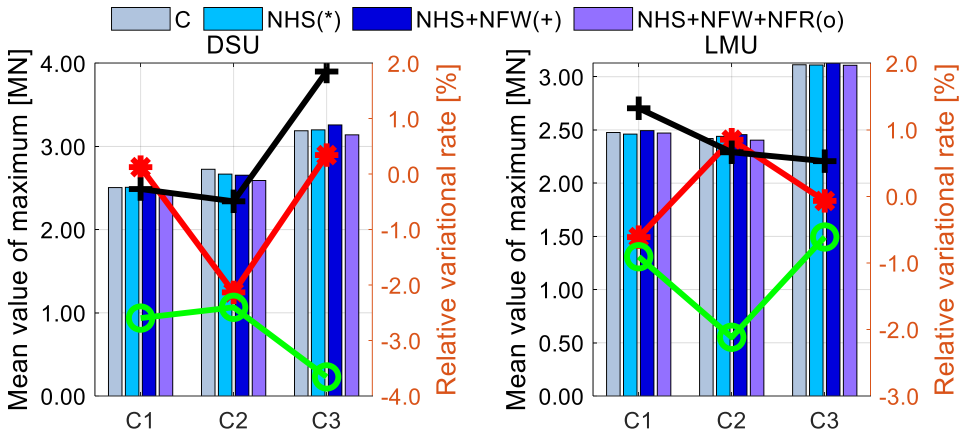

Fig. 20. Statistical vertical forces of DSU and LMU in beam sea

6. Conclusion

The present study develops a numerical modeling method to calculate nonstationary hydrodynamic forces and induced responses for simulation of continuous offshore installations, where a continuous update of the body boundary conditions for hydrodynamic analysis is occurred. Targeting the load transfer operation for FOD installation, the proposed method is used to calculate the quasistatic motions of the barge first, and then the effects of time varying body boundary conditions on the different hydrodynamic forces are discussed. The corresponding effects on the induced motions and the contact loads are also investigated. Some conclusions can be drawn from the study.

(a) In quasistatic analysis, a panel model with improved efficiency is developed to calculate the time varying buoyancy of the floating body with a nonlinear method based on the integration of hydrostatic pressure considering the instantaneous position/inclination of the barge. The results show that it is important to capture the nonlinear relationships between buoyancy and displacement when the mean water plane of the floating body is largely changed.

(b) The quasistatic motions induced inertial force are defined representing the operation induced dynamic forces. Larger motions are observed at the end of the load transfer operation, that indicates it plays an important role for analysis.

(c) The hydrodynamic forces, barge motions and contact forces show same change tendency under the effects of time varying body boundary conditions. However, the changes of these nonstationary responses are little during the load transfer operation. When the load transfer ended, larger effects on the hydrodynamic forces, motions and contact forces are observed. It could be recommended that the dynamic analysis of the rapid load transfer operation for FOD installation can be effectively carried out with one update of hydrodynamic forces at the end of the operation.

(d) For different wave period, there is a minimum effect of time varying body boundary conditions on heave, pitch and roll wave excitation forces and motions with condition of long period waves.

(e) The results show that the barge roll motions including its natural period and amplitude are the most affected with consideration of the time varying body boundary conditions, which should be carefully considered in offshore operation.

The developed methodology is stimulated by the demand from the huge platform integration/decommission as well as the offshore wind turbine installation activities, where there are wet surface variations with the rapid load transfer at critical mating operation stage. For the sake of simplicity, the drift motions caused by the second-order wave forces are ignored. Further research work on it and the intensive experimental validations needs to be done in the future.

Acknowledgments

The work is supported by the National Natural Science Foundation of China (No. 52088102 and No.52071307).

References

Ansys, A., 2013. Theory manual. ANSYS Inc., Canonsburg, PA, USA.

Bai, X.-d., Luo, H.-b., Xie, P., 2021. Effect of Wave Headings on the Dynamic Response of the Continuous Mating Operation of Floatover Installation. China Ocean Engineering 35 (1), 72-83.

Bai, X., Luo, H., Xie, P., 2020a. Experimental analysis of dynamic response of floatover installation using rapid transfer technique in continuous load transfer process. Journal of Marine Science and Technology 25 (4), 1182-1198.

Bai, X., Luo, H., Xie, P., 2020b. Experimental investigation on motions behavior and loads characteristic of floatover installation with T-shaped barge. Ocean Engineering 195, 106761.

Chen, M., Eatock Taylor, R., Choo, Y.S., 2017. Investigation of the complex dynamics of float-over deck installation based on a coupled heave-roll-pitch impact model. Ocean Engineering 137, 262-275.

Cummins, W., 1962. The impulse response function and ship motions. David Taylor Model Basin Washington DC.

Faltinsen, O., 1993. Sea loads on ships and offshore structures. Cambridge university press.

Garrett, D., 1982. Dynamic analysis of slender rods.

Koo, B., Magee, A., Lambrakos, K., Beyko, E., Sablok, A., 2010a. Model tests for floatover installation of spar topsides, International Conference on Offshore Mechanics and Arctic Engineering, pp. 363-371.

Koo, B., Magee, A., Lambrakos, K., Beyko, E., Sablok, A., 2010b. Prediction of motions and loads for floatover installation of spar topsides, International Conference on Offshore Mechanics and Arctic Engineering, pp. 373-386.

Li, L., Gao, Z., Moan, T., 2015. Response analysis of a nonstationary lowering operation for an offshore wind turbine monopile substructure. Journal of Offshore Mechanics and Arctic Engineering 137 (5).

Lin, W.M., 1990. Numerical Solutions for Large-Amplitude Ship Motions in the Time Domain, Prec. 18th Symposium on Naval Hydrodynamics.

Liu, G., Li, H., 2017. Offshore platform integration and floatover technology. Springer.

MARINTEK, 2012. SIMO—Theory Manual Version 4.0. Marintek Trondheim, Norway.

Nachlinger, R., 2013. Reference Manual for MOSES. Ultramarine. Inc.

O'neill, L., Fakas, E., Ronalds, B., Christiansen, P., 2000. History, trends and evolution of float-over deck installation in open waters, SPE Annual Technical Conference and Exhibition. Society of Petroleum Engineers.

Ogilvie, T.F., 1964. Recent progress toward the understanding and prediction of ship motions, 5th ONR Symp. on Naval Hydrodynamics.

Orihara, H., Miyata, H., 2003. A numerical method for arbitrary ship motions in arbitrary wave conditions using overlapping grid system, 8th Int. Conf. Numer. Ship Hydro., Busan, Korea.

Taghipour, R., Perez, T., Moan, T., 2008. Hybrid frequency–time domain models for dynamic response analysis of marine structures. Ocean Engineering 35 (7), 685-705.

Wadam, D., 2010. Wave analysis by diffraction and Morison theory. SESAM user manual. Det Norske Veritas, Høvik.

Yu, W., Wang, A.M., Zhu, S., Xu, J., Wang, A., Luo, H., 2018. Rapid load transfer technology for floatover installations, The 28th International Ocean and Polar Engineering Conference. International Society of Offshore and Polar Engineers.

Zhao, S., Meng, X., Li, H., Li, D., Fu, Q., 2021. Continuous multi-body dynamic analysis of float-over deck installation with rapid load transfer technique in open waters. Ocean Engineering 224, 108729.